L-band Overhauser dynamic nuclear polarization

Sandra Garcia [a,*], Jeffrey H. Walton [b], Brandon Armstrong [c], Songi Han [d], Michael J. McCarthy [a]

[a] *Department of Food Science & Technology, University of California, Davis, CA 95616, USA*
[b] *UCD NMR Facility, University of California, Davis, CA 95616, USA*
[c] *Department of Physics, University of California, Santa Barbara, CA 93106, USA*
[d] *Department of Chemistry and Biochemistry, University of California, Santa Barbara, CA 93106, USA*

ARTICLE INFO

ABSTRACT

We present the development of an Overhauser dynamic nuclear polarization (DNP) instrument at 0.04 T using 1.1 GHz (L-band) electron spin resonance frequencies (ESR) and 1.7 MHz ^{1}H nuclear magnetic resonance frequencies. Using this home-built DNP system, the electron–nucleus coupling factor of 4-oxo-TEMPO dissolved in water was determined as 0.39 ± 0.06 at 0.04 T. The higher coupling factor obtained at this field compared to higher magnetic fields, such as 0.35 T, directly translates to higher enhancement of the NMR signal and opens up a wider time scale window for observing water dynamics interacting with macromolecular systems, including proteins, polymers or lipid vesicles. The higher enhancements obtained will facilitate the observation of water dynamics at correlation times up to 10 ns, that corresponds to more than one order of magnitude slower dynamics than accessible at 0.35 T using X-band ESR frequencies.

1. Introduction

NMR is a powerful analytical technique that provides molecular level and macroscopic information about a vast array of systems. A limitation of NMR, when compared with other analytical techniques is its relative insensitivity. Thus, one of the greatest developmental needs is to advance NMR analysis beyond the current limits by enhancing the sensitivity and signal contrast between different (molecular) environments. In recent years, there has been significant effort to develop hyperpolarization techniques that overcome some of these inherent limitations. Methods such as the hyperpolarization of noble gases by optical pumping (^{129}Xe, ^{3}He, and ^{83}Kr) [1–4], PASADENA [5,6], and dynamic nuclear polarization (DNP) [7] have each been used for specific purposes and systems. DNP in particular has been noted for providing enhancements of 2–3 orders of magnitude, and is accomplished by transferring the much higher spin polarization of the electron to the nucleus. Several mechanisms of enhancement exist, such as the solid effect [7,8], thermal mixing [7], cross effect [9] and Overhauser mechanism [10,11]. Most applications for DNP occur at high fields and utilize one of the first three mechanisms mentioned. These mechanisms require freezing the sample and benefit from specially synthesized radicals [12]. The large gains in signal also come with great instrumentation costs. The Overhauser effect, on the other hand, is straight forward to implement because it can be carried out in solution state and at lower magnetic fields with less demanding hardware requirements. The loss of meaningful ^{1}H chemical shift dispersion that occurs from performing Overhauser DNP experiments at low magnetic fields can be overcome by shuttling the sample to a higher field, where chemical shift dispersion is available [13–16] This work focuses on developing an instrument to carry out Overhauser DNP using L-band electron spin resonance frequencies at 0.04 T, and to discuss potential merits of L-band versus X-band Overhauser DNP capabilities, as reflected in the different coupling factors between nitroxide radicals and water at 0.04 T versus 0.35 T fields.

Overhauser DNP occurs when irradiating the unpaired electron with radiation at its resonance frequency. The electron and the nuclear spins are dipolar and/or scalar coupled through a motion-mediated cross relaxation process. Thus, as the electron spins are saturated, i.e., driven out of equilibrium, the electron spin flips drive nuclear spin flips, effectively transferring the electron's higher spin polarization into nuclear spin polarization. A literature review shows that Overhauser DNP is utilized at a wide range of magnetic fields. Two early reviews show work occurring at 0.0016, .018, 0.11, 0.35 and 1.36 T [11,17], while more recent literature brings up work that includes Earth's field [18], 0.35 T [19–21], 3.3 T [22] and 9.2 T [23]. Nitroxide radicals are commonly used as the source of electron spins because of their stability and non-reactivity [13–15,24,25]. At ultra-low field, the low signal resulting from low spin polarization makes signal enhancement through DNP a very attractive choice, as was shown by Halse and Callaghan [18]. Because electronic transitions that

* Corresponding author.
  E-mail address: spgarcia24@gmail.com (S. Garcia).

become forbidden at higher fields are allowed at ultra-low fields and the hyperfine coupled field becomes much greater than the main magnetic field, enhancements on the order of 3000 relative to thermal polarization of water become possible [26]. At 9.2 T, an enhancement factor of −14 over thermal polarization of water signal was reported [23]. Although this seems like a very modest gain, the availability of chemical shift information and the possibility of transferring polarization from the solvent to larger biological systems makes DNP at 9.2 T potentially very attractive. For 0.35 T, experimental enhancements of up to −140 have been reported by Höfer et al. [21]. A novel assortment of experiments that uniquely and sensitively probe the internal water dynamics of lipids, proteins and coacervates in the 0.1–0.5 ns correlation timescale has been successfully carried out at 0.35 T [20,27–29]. Further explanation of this time scale is provided in Section 2. These experiments do not require chemical shift dispersion, indicating that useful chemical information at the molecular level is available even at 0.04 T, where no meaningful ^{1}H chemical shift information is available without shuttling the sample to higher fields.

The underlying factor that determines the magnitude of enhancements at each of the above mentioned fields is the coupling factor between the electron and the nucleus that critically depends on the magnetic field. The coupling factor approaches 0.5 for dipolar and −1 for scalar interactions at low magnetic field [11]. The size of the coupling factor depends on the motion of the two spin-bearing molecules. The faster the translational (or rotational) motion of the molecule to be hyperpolarized with respect to the electron spin Larmor frequency, the larger the coupling factor. DNP has proven to be an insightful tool for quantifying water dynamics in and around proteins, lipid vesicles or polymer complexes. By placing a nitroxide spin label at specific sites of the molecule or soft matter, local water dynamics within 10 Å of the spin label site can be quantified. Conventionally, local and surface water dynamics is not amenable to NMR analysis of dilute molecular systems in bulk water. Overhauser DNP at 0.35 T is particularly effective for dynamic water that is translating with correlation times of 0.5 ns or less with respect to the (free or tethered) spin label. However, when the spin label is located inside a hydrophobic core resulting from protein folding or aggregation, or tight macromolecular complexation, the dynamics of local water may slow beyond 0.5 ns, and thus provide negligible enhancements at 0.35 T. By decreasing the magnetic field strength to 0.04 T where the electron spin resonance frequency is an order of magnitude lower, molecules (in this case ^{1}H bearing water) that are moving too slow to provide Overhauser enhancement at 0.35 T, may give appreciable enhancements at 0.04 T. To investigate and utilize these characteristics of higher enhancement figures and thus larger coupling factors, a DNP polarizer that operates at 0.04 T was built. A field of 0.04 T corresponds to an NMR frequency of 1.7 MHz and ESR frequency of 1.12 GHz (i.e., L-band). At both of these frequencies, electronic components including capacitors, amplifiers and mixers are readily available off the shelf.

Details of the construction of an L-band DNP polarizer and its applications to measure the coupling factor and hydration dynamics are reported. The approach of Armstrong and Han [19,20] is used to quantify the electron–nucleus coupling factor.

2. Theory

The general equation for Overhauser DNP enhancement is given by

$$E = 1 - \rho f s \frac{|\gamma_S|}{\gamma_I} \tag{1}$$

where ρ is the coupling factor between the electron and the nucleus and

$$f = 1 - \frac{T_1}{T_{10}} = \frac{kCT_{10}}{1 + kCT_{10}}. \tag{2}$$

f is the leakage factor that describes the electron's ability to relax the nucleus. T_1 and T_{10} are the spin lattice relaxation times of the solvent with and without radical, respectively. f can also be expressed in terms of concentration, C, and the relaxivity constant, k. Eq. (2) shows that the leakage factor approaches 1 at high radical concentrations. The saturation factor, s, is a function of radiation power driving the electron spin transitions. The three ESR lines in nitroxide radicals caused by the hyperfine coupling of the electron and ^{14}N nucleus make the determination of this parameter complicated. Heisenberg spin exchange occurring between the three nitroxide lines mixes the states; thus, irradiation of one line results in non-equilibrium of the other two states. Heisenberg spin exchange is dependent on concentration and results in adding a concentration term to the saturation factor [19,30]. To account for the mixing of the three states, when only one line is irradiated, the enhancement can be measured as a function of power and extrapolated to infinite power,

$$E_{\max} = E(P \to \infty) = 1 - \frac{\omega_S}{\omega_I} \rho f s_{\max}. \tag{3}$$

where ω_S and ω_I are the frequency of irradiation of the electron and nucleus, respectively and

$$s_{\max} = \frac{1}{3} \left(\frac{1 + 3k'C/p}{1 + k'C/p} \right). \tag{4}$$

k' and p are the Heisenberg exchange rate and $1/T_{1e}$ of the electron, respectively. The 1/3 factor that arises because of the hyperfine splitting of the electron and ^{14}N nucleus is removed by taking the limit of Eq. (4) at high concentration, $s_{\max}(C \to \infty) = 1$. Since both f and $s_{\max}$ approach 1 at high radical concentration $E_{\max}$ can be expressed as:

$$E_{\max}(C \to \infty) = 1 - \frac{\omega_S}{\omega_I} \rho. \tag{5}$$

This final equation shows that if the enhancement is measured as a function of concentration, the coupling factor, ρ, can be directly determined from experimental data without further need for modeling or assumptions on molecular dynamics models. It should be noted that while reference 19 predicts the maximum possible saturation factor to increase with radical concentration, the actual measured DNP enhancements will also depend on linewidth. A thorough study of saturation factor taking into account the full electron spin relaxation matrix is presented by Sezer et al. [31]. The analysis by Sezer et al., concludes that Heisenberg spin exchange effects increase measured DNP enhancements.

The determination of the translational correlation time, τ, of water diffusion from the measured coupling factor, however, requires the use of appropriate molecular dynamics and relaxation models. Using the force free, hard sphere model [32,33], and assuming dipolar coupling, the translational correlation time, τ, can be calculated from the coupling factor [11,19] according to the following equation:

$$\rho = \frac{6J(\omega_S + \omega_I, \tau) - 6J(\omega S - \omega I, \tau)}{6J(\omega I + \omega S, \tau) + 3J(\omega I, \tau) + J(\omega S - \omega I, \tau)}. \tag{6}$$

where the spectral density is given by:

$$J(\omega, \tau) = \frac{1 + \frac{5\sqrt{2}}{8}(\omega\tau)^{1/2} + \frac{\omega\tau}{4}}{1 + (2\omega\tau)^{1/2} + (\omega\tau) + \frac{\sqrt{2}}{3}((\omega\tau)^{3/2}) + \frac{16}{81}(\omega\tau)^2 + \frac{4\sqrt{2}}{81}(\omega\tau)^{5/2} + \frac{(\omega\tau)^3}{81}}. \tag{7}$$

The coupling factor's sensitivity to the translational motion as well as to the magnetic field under which the system is studied is evident as shown in Fig. 1, where Eq. (6) is plotted for a range of correlation times at 0.35 and 0.04 T. The correlation time is associated with the summed diffusion coefficient of the radical and water, D, that can be obtained through the relationship $\tau = d^2/D$, where d is the distance of closest approach between the proton of water and the unpaired electron of the radical. For 0.35 T, the coupling factor approaches zero as the translational correlation time exceeds 0.5 ns, while for 0.04 T the coupling factor approaches zero at a correlation time beyond 10 ns.

3. Experimental

3.1. Samples

The free radical 4-oxo-TEMPO was purchased from Sigma–Aldridge. Solutions were made by first preparing a 0.4 M solution of 4-oxo-TEMPO in deuterated dimethylsulfoxide, d-DMSO. A 0.02 M solution in D.I. water was then prepared as a stock solution. All samples were prepared from this stock solution. Approximately 100 μL of sample was used for each measurement.

3.2. Experimental setup

A schematic of the polarizer is shown in Fig. 2. The electrical components shown in the schematic are listed in Table 1. (Note: The design could be simplified by substituting an L-band frequency source for components starred in Table 1.) The B_0 field is produced by a 0.04 T permanent magnet of Halbach design (Quantum Magnetics, San Diego, CA). A KEA spectrometer (Magritek, New Zealand) is used to control both the microwave (MW) and the radio frequency RF source. An experiment consisted of switching on the MW via a TTL pulse from the KEA spectrometer, irradiating the sample for at least $5 * T_1$ of the water protons then acquiring the NMR signal while still irradiating the sample with the MW source. The maximum output power of the MW source is 30 W. For samples with high radical concentrations, the output power of the amplifier was set to approximately 6 W. For samples with low radical concentrations, the output was set to 4 W. The requirement to employ higher MW power for the saturation of ESR lines results from broadening of the lines due to Heisenberg spin exchange effects. A probe was constructed to accommodate both the ESR and NMR circuit as shown in Fig. 3. The ESR circuit's tuning capabilities span the frequency range of the radical from 1.05 to

1.19 GHz, albeit the Q of the coil was not constant over this frequency range. The ESR circuit is composed of a tuning and matching capacitor (polyflon, 0.8–10 pf) and a loop-gap resonator. The loop-gap resonator is made of copper sheet (1 cm height, 0.7 cm diameter) and has two rows and two columns of 1 pf chip capacitors spanning the gap and distributing the charge over the resonator. The NMR circuit is tank circuit composed of a tuning and matching capacitor (Voltronics, 2–120 pf) and a solenoid coil (1 cm height, 1.5 cm diameter, 35 gauge wire). The NMR circuit is stably tuned to 1.7 MHz with a Q of 260. A sample with up to 5 mm diameter is placed in the overlapping region of the loop-gap resonator and the solenoid coil. Doty susceptibility plugs (Wilmad Labglass, Buena, NJ) were used to constrain the sample to the region of homogeneous RF and MW radiation.

3.3. Data processing

All NMR spectra were acquired and processed using PROSPA (Magritek, New Zealand). E_{max} values were obtained by plotting enhancement as a function of power and fitting the curves to the equation $E_{max} = 1 - AP/(1 + BP)$. E_{max} can then be calculated by $E_{max} = 1 - A/B$. T_{10} and T_1 were measured for each concentration using saturation recovery with echo acquisition and used to calculate the leakage factor, f, at each concentration. These results were then fit to Eq. (2) to determine k. All fits were performed using MatLab's curve fitting toolbox (Matlab™ Version 2008b, The Mathworks, Naticle, MA).

4. Results and discussion

Fig. 4a shows the proton spectra for a water sample containing 4-oxo-TEMPO (14 mM) without enhancement and with enhancement (79% saturation of ESR signal). Fig. 4b is the ESR spectrum of the radical measured indirectly by using the Overhauser enhancements through the proton NMR signal at 40% saturation of the ESR signal. Here, the enhancements observed at 14 mM radical concentrations were utilized to probe the ESR spectrum by varying the frequency of the MW source. The maximum enhancements occurred at 1075, 1121 and 1166 MHz, reflecting the known hyperfine splitting of 45 MHz. The absolute value of the enhancement was largest at 1121 MHz, decreasing at 1166 Hz and 1075 MHz. Theory predicts (Eqs. ((refspseqn3)–(5))) that the enhancement should increase with increasing ESR frequency. This deviation from theory in the indirect ESR spectrum is a result of a non-constant Q of the loop-gap resonator over the frequency range of 1060–1180 MHz. We proceeded to calculate the coupling factor by measuring enhancements using the lower frequency of 1075 MHz of the ESR hyperfine line as the irradiation frequency. The loop-gap circuit was very stable at this frequency ensuring consistent power delivery when samples were changed. Care was taken to prevent sample heating at high MW powers by providing ample rest time between successive MW irradiations. Although the experimental data nicely fits our assumptions, we still cannot entirely ignore the possibility of sample heating which can skew our measurements and analysis. The issue of sample heating and its effect on DNP measurements is currently under investigation.

Table 2 shows a summary of the experimental enhancements, $E_{measured}$, as well as the enhancements extrapolated to infinite power, E_{max}. At low concentration, $E_{measured}$ was very close to the E_{max} value, signifying almost complete saturation. The saturation can be quantified by calculating $s_{measured}$ with Eq. (1) and s_{max} with Eq. (3) using 0.39 as the coupling factor and the measured value of f that is also listed in the table. Nearly complete saturation is obtained at low radical concentrations while at higher concentration significantly less saturation is achieved. This result was expected
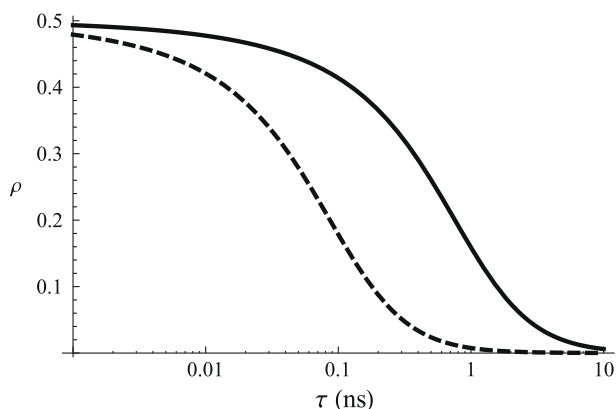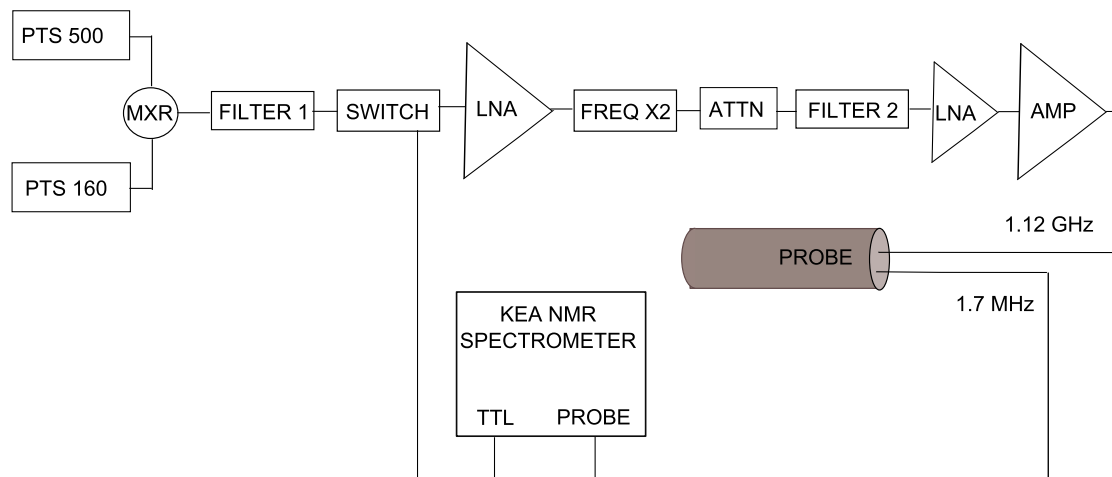

Fig. 1. Plots of Eq. (6) for 0.35 T (dashed line) and 0.04 T (solid line). The coupling factor, ρ, is sensitive to the motional timescales at the two magnetic fields. The coupling factor approaches zero at much shorter translational correlation times (0.5 ns) at 0.35 T than at 0.04 T (10 ns).
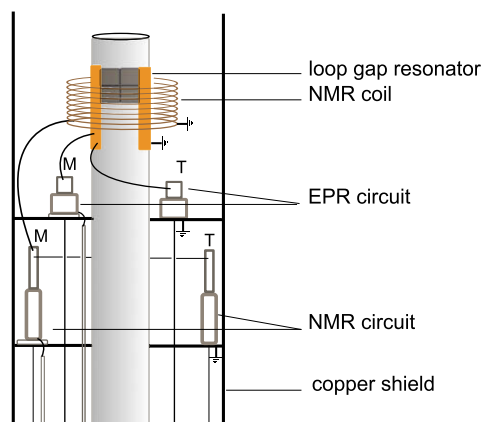
Fig. 2. A block diagram of DNP setup. The MW source is produced by mixing the frequency of a PTS500 with a PTS160 then doubling the summed frequency to achieve ~1 GHz. The frequency of both PTSs can be varied to obtain the desired output between 1.050 and 1.190 GHz.

Table 1
List of components making up the L-band frequency source. The components marked with [a] could be replaced using a single L-Band frequency source.
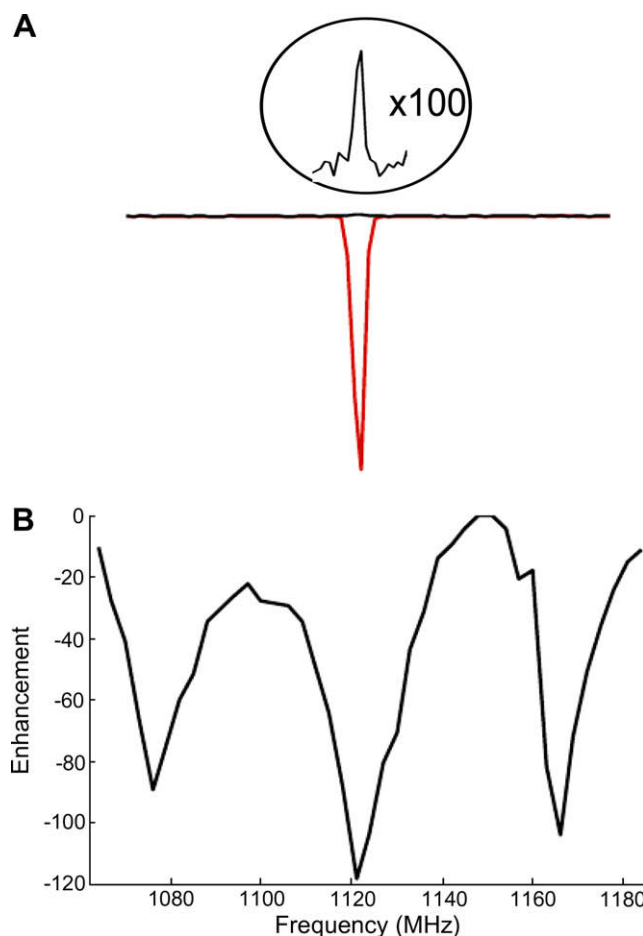
	Description	Manufacturer	Model
PTS 500[a]	Frequency synthesizer	Programme Test Source Inc.	500-B7010
PTS 160[a]	Frequency synthesizer	Programmed Test Source Inc.	160-R7N10
MXR[a]	Frequency mixer	Minicircuits	ZFM-4
FILTER 1[a]	High pass filter	Minicircuits	BHP-500+
SWITCH	TTL triggered switch	Minicircuits	ZSDR-230+
LNA[a]	Low noise amplifier	Minicircuits	ZRL-3500
FREQ X2[a]	Frequency doubler	Minicircuits	FK-3000
ATTN	Rotary attenuators	JFW	50BR-08
FILTER 2	High pass filter	Minicircuits	SHP-1000+
LNA	Low noise amplifier	Minicircuits	ZRL-3500
AMP	30 W amplifier	Minicircuits	ZWL-30W-252-S+

Fig. 3. DNP probe. The ESR and NMR circuits are housed in the same probe.

Fig. 4. (A) Spectra of 14 mM, 4-amino-TEMPO in water with MW irradiation (black) and without (red). The water signal is enhanced by a factor of −150 upon MW irradiation. The unenhanced signal was magnified by two orders of magnitude for spectral clarity. (B) The intensity of DNP enhancement was measured as a function of ESR frequency. Note that enhancements are negative. (For interpretation of the references to colour in this figure legend, the reader is referred to the web version of this article.)

since it is increasingly difficult to achieve complete saturation at higher radical concentrations where the ESR lines are broadened by spin exchange effects. Nonetheless, s_{max} of 0.8 was attained for a 14 mM radical concentrations.

The dependence of the DNP enhancement factor on the nitroxide radical concentration was measured, and is plotted in Fig. 5. For a series of samples with differing nitroxide concentration, E_{max} was measured as a function of MW power for each sample, and the data extrapolated to infinite power, as shown in Fig. 6. When the data given in Fig. 5 is fit to relations given in Eq. (3) and the expression for s_{max} given in Eq. (4), the result is $\rho = 0.39 \pm 0.06$ and $k'/p = 0.16 \pm 0.1$. This is the first determination of the electron–

Table 2
Summary of DNP experimental results and calculations.

Conc. (mM)	$E_{measured}$	E_{max}	$s_{measured}$	s_{max}	% saturation	T_1 (ms)	f
D.I. H$_2$0						2230	0
0.5	−29.3	−30.9	0.38	0.42	91	1543	0.31
1	−44.8	−47.8	0.41	0.46	90	1273	0.43
2	−68.6	−72.3	0.41	0.45	91	767	0.67
4	−82.1	−113.6	0.43	0.61	70	532	0.76
6	−123.7	−136.1	0.57	0.65	88	318	0.86
8	−144.3	−161.1	0.64	0.74	86	265	0.88
10	−141.4	−161.2	0.61	0.73	84	229	0.90
12	−142.1	−174.6	0.60	0.77	78	158	0.93
14	−150.1	−182.4	0.63	0.8	79	151	0.93
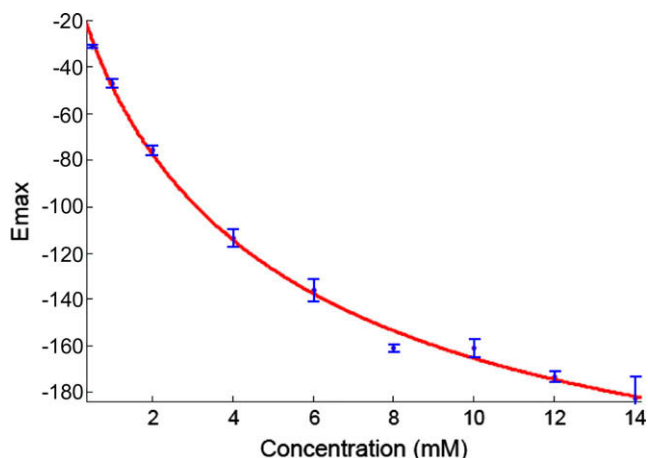
Fig. 5. Emax values used to determine ρ. A fit of the data (red line) gave $\rho = 0.39 \pm 0.06$. (For interpretation of the references to colour in this figure legend, the reader is referred to the web version of this article.)
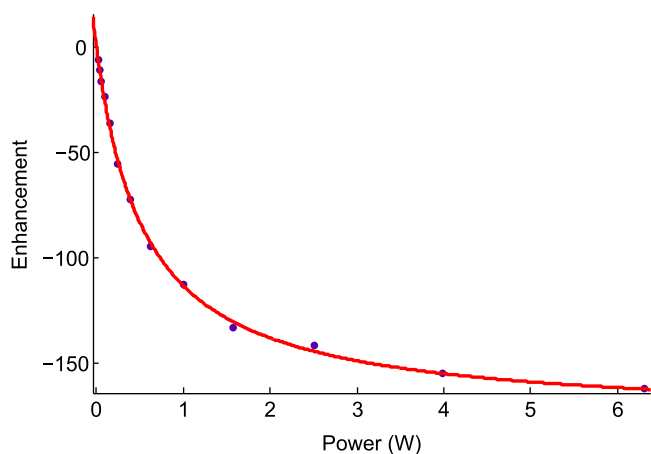
Fig. 6. Enhancement of aqueous solutions with 14 mM 4-oxo-TEMPO as a function of increasing MW power. The maximum power employed was approximately 6 W. The fitted curve extrapolates to an enhancement of −182-fold.

nucleus coupling factor at 0.04 T. The maximum value for pure dipolar coupling is predicted to be 0.5 [11]. Experimental data and molecular dynamic simulations suggest that electron–nucleus coupling for nitroxide radicals in water is dominated by dipolar interactions [17,34], although a small but non-negligible amount of scalar coupling may be present [34,35].

The translational correlation time of 76 ps determined at 0.35 T [20] can be used to predict the coupling factor a field of 0.04 T. Such an analysis gives an expected coupling factor of 0.43 which is somewhat larger, but still within the error of the experimentally deter-

mined value of 0.39 ± 0.06. However, coupling factors obtained at 0.35 T through different methodological approaches have yielded different results. For example, both Höfer et al. and Armstrong and Han have reported on a coupling factor of 0.36 at 0.35 T and τ of 25 ps for a similar nitroxide system using field cycling relaxometry analysis, presenting distinctly different results obtained from Overhauser DNP measurements [20,22]. If this correlation time of 25 ps is used in Eqs. (6) and (7), ρ is estimated as 0.46 at 0.04 T, which would be a value approaching the dipolar limit. Then, experimental enhancements on the order of −300 should be possible with this ρ. However, the highest measured enhancement was thus far −150, which is only half of the value as predicted from the field cycling relaxometry analysis. Also, molecular dynamics simulations predict a coupling factor of 0.296 [34]. The presence of a scalar contribution would result in the coupling factor being smaller than predicted. One possibility to rule out the contributions of scalar coupling is to perform DNP experiments at a lower field than 0.04 T to confirm that the dipolar limit of the coupling factor, 0.5, is reached [11,13]. Currently, the discrepancy between the three coupling factors (.22, .36 and .296) at 0.35 T is unresolved and has yet to be fully explained. However, the important use of an L-band instrument is the ability of accessing higher ^{1}H NMR enhancement factors as compared to higher magnetic field based systems. The higher coupling factor at L-band implies that water dynamics with more than an order of magnitude slower correlation times (0.1–10 ns) as compared to the times accessible at X-band (.01–0.5 ns).

5. Conclusion

An electron–nucleus coupling factor of 0.39 ± 0.06 was measured for aqueous solutions of 4-oxo-TEMPO. This was the first L-band measurement of the electron–nucleus coupling factor. Although DNP via the Overhauser effect is commonly employed at various fields, the quantitative employment of the coupling factor and their application to the characterization of hydration dynamics of macromolecules occurs mainly at 0.35 T fields. With the increased interest in Overhauser DNP analysis and the discrepancies in coupling factors found by different groups and experimental approaches, an additional data point for the coupling factor at 0.04 T is valuable for improving the theoretical understanding of the Overhauser DNP. Ultimately, quantification of the coupling factor and the employment of the appropriate dynamic model will allow for the quantification of local hydration dynamics within 10 Å of specifically localized spin labels on the surface of macromolecules or molecular assemblies. Surface and interfacial hydration dynamics is an essential parameter for probing intermolecular interaction, such as in protein folding or lipid vesicle fusion. Of particular importance is that the larger ρ at 0.04 T will provide a much wider time window (>0.5 ns) for probing dynamics of hydration water, including structural and bound water, that interact with these complex molecular systems.

References

[1] B.M. Goodson, Nuclear magnetic resonance of laser-polarized noble gases in molecules, materials, and organisms, J. Magn. Reson. 155 (2002) 157.

[2] L. Schroeder, T.J. Lowery, C. Hilty, D.E. Wemmer, A. Pines, Molecular imaging using a targeted magnetic resonance hyperpolarized biosensor, Science 314 (2006) 446–449.

[3] G.E. Pavlovskaya, Z.I. Cleveland, K.F. Stupic, R.J. Basaraba, T. Meersmann, Hyperpolarized krypton-83 as a contrast agent for magnetic resonance imaging, Proc. Natl. Acad. Sci. USA 102 (2005) 18275–18279.

[4] M.S. Conradi, B.T. Saam, D.A. Yablonskiy, J.C. Woods, Hyperpolarized ^{3}He and perfluorocarbon gas diffusion MRI of lungs, Prog. NMR Spectrosc. 48 (2006) 63–83.

[5] E.Y. Chekmenev, J. Hövener, V.A. Norton, K. Harris, L.S. Batchelder, P. Bhattacharya, B.D. Ross, D.P. Weitekamp, PASADENA hyperpolarization of succinic acid for MRI and NMR spectroscopy, J. Am. Chem. Soc. 130 (2008) 4212–4213.

[6] M. Goldman, H. Jóhannesson, O. Axelsson, M. Karlsson, Hyperpolarization of ^{13}C through order transfer from parahydrogen: a new contrast agent for MRI, Magn. Reson. Imaging 23 (2005) 153.

[7] T. Maly, G.T. Debelouchina, V.S. Bajaj, K.N. Hu, C.G. Joo, M.L. Mak-Jurkauskas, J.R. Sirigiri, P.C.A. van der Wel, J. Herzfeld, R.J. Temkin, R.G. Griffin, Dynamic nuclear polarization at high magnetic fields, J. Chem. Phys. 128 (2008) 052211.

[8] W.T. Wenckebach, The solid effect, Appl. Magn. Reson. 34 (2008) 227–235.

[9] K.-N. Hu, C. Song, H.-H. Yu, T.M. Swager, R.G. Griffin, High-frequency dynamic nuclear polarization using biradicals: a multifrequency EPR lineshape analysis, J. Chem. Phys. 128 (2008) 052301-1-7.

[10] T.R. Carver, C.P. Slichter, Polarization of nuclear spins in metals, Phys. Rev. 92 (1953) 212.

[11] K.H. Hausser, D. Stehlik, Dynamic nuclear polarization in liquids, Adv. Magn. Reson. 3 (1968) 79.

[12] C. Song, K.-N. Hu, C.-G. Joo, T.M. Swager, R.G. Griffin, TATOPOL: a biradical polarizing agent for dynamic nuclear polarization experiments in aqueous media, J. Am. Chem. Soc 128 (2006) 11385–11390.

[13] R. Gitti, C. Wild, C. Tsiao, k. Zimmer, T.E. Glass, H.C. Dorn, Solid-liquid intermolecular transfer of dynamic nuclear polarization. Enhanced flowing fluid 1H NMR signals via immobilized spin labels, J. Am. Chem. Soc 110 (1988) 2294–2296.

[14] K.H. Tsai, H.C. Dorn, A model for establishing the ultimate enhancements (A_Y) in the low to high magnetic field transfer dynamics nuclear polarization experiment, Appl. Magn. Reson. 1 (1990) 231–254.

[15] H.C. Dorn, T.E. Glass, R. Gitt, T.H. Tsai, Transfer of ^{1}H and ^{13}C dynamic nuclear polarization from immobilized nitroxide radicals and flowing liquids, Appl. Magn. Reson. 2 (1991) 9–27.

[16] M. Reese, M.T. Türke, I. Tkach, G. Parigi, C. Luchinat, T. Marquardsen, A. Tavernier, P. Höfer, F. Engelke, C. Griesinger, M. Bennati, "1H and 13C dynamic nuclear polarization in aqueous solution with a two-field (0.35 T/14T) shuttle DNP spectrometer, J. Am. Chem. Soc. 131 (2009) 15086–15087.

[17] W. Muller-Warmuth, K. Meise-Gresch, Molecular motions and interactions as studied by dynamic nuclear polarization (DNP) in free radical solutions, Adv. Magn. Reson. 11 (1983) 1–45.

[18] M.E. Halse, P.T. Callaghan, A dynamic nuclear polarization strategy for multi-dimensional Earth's field NMR spectroscopy, J. Magn. Reson. 195 (2008) 162–168.

[19] B.D. Armstrong, S. Han, A new model for Overhauser enhanced nuclear magnetic resonance using nitroxide radicals, J. Chem. Phys. 127 (2007) 104508.

[20] B.D. Armstrong, S. Han, Overhauser dynamic nuclear polarization to study local water dynamics, J. Am. Chem. Soc. 131 (2009) 4641–4647.

[21] P. Höfer, P. Carl, G. Guthausen, T. Prisner, M. Reese, T. Carlomagno, C. Griesinger, M. Bennati, Studies of dynamic nuclear polarization with nitroxides in aqueous solution, Appl. Magn. Reson. 34 (2008) 393–398.

[22] P. Höfer, G. Parigi, C. Luchinat, P. Carl, G. Guthausen, M. Reese, T. Carlomagno, C. Griesinger, M. Bennati, Field dependent dynamic nuclear polarization with radicals in aqueous solution, J. Am. Chem. Soc. 130 (2008) 3254–3255.

[23] M.J. Pranholini, V.P. Denysenkov, M. Gafurov, B. Endewar, T.F. Prisner, High-field dynamic nuclear polarization in aqueous solutions, J. Am. Chem. Soc. 131 (2009) 6090–6092.

[24] E.R. McCaney, S. Han, Spin-labeled gel for the production of radical free dynamic nuclear polarized enhanced molecules for NMR spectroscopy and imaging, J. Magn. Reson. 192 (2008) 307–315.

[25] J.L. Russ, J. Gu, K.-H. Tsai, T. Glass, J.C. Duchamp, H.C. Dorn, Nitroxide/substrate weak hydrogen bonding: attitude and dynamics of collisions in solution, J. Am. Chem. Soc. 129 (2007) 7018–7027.

[26] T. Guiberteau, D. Grucker, Dynamic nuclear polarization of water protons by saturation of σ and π EPR transitions of nitroxides, J. Magn. Reson. Ser. A 105 (1993) 98–103.

[27] E.R. McCarney, B.D. Armstrong, R. Kausik, S. Han, Dynamic nuclear polarization enhanced nuclear magnetic resonance and electron spin resonance studies of hydration and local water dynamics in micelle and vesicle assemblies, Langmuir 24 (2008) 10062–10072.

[28] A. Pavlova, E.R. McCarney, D.W. Peterson, F.W. Dahlquist, J. Lew, S. Han, Phys. Chem. Chem. Phys. 11 (2009) 6833–6839.

[29] R. Kausik, A. Srivastava, P.A. Korevaar, G. Stucky, J.H. Waite, S. Han, Local water dynamics in coacervated polyelectrolytes monitored through dynamic nuclear polarization-enhanced ^{1}H NMR, Macromolecules 42 (2009) 7404–7412.

[30] R.D. Bates Jr., W.S. Drozdoski, Use of nitroxide spin labels in studies of solvent–solute interactions, J. Chem. Phys. 67 (1977) 4038–4044.

[31] D. Sezer, M. Gafurov, M.J. Prandolini, V.P. Denysenkov, T.F. Prisner, Dynamic nuclear polarization of water by a nitroxide radical: rigorous treatment of the electron spin saturation and comparison with experiments at 9.2 T, Phys. Chem. Chem. Phys. 11 (2009) 6638–6653.

[32] J.H. Freed, Dynamic effects of pair correlation functions on spin relaxation by translational diffusion in liquids. II. Finite jumps and independent T_1 processes, J. Chem. Phys. 68 (1978) 4034–4037.

[33] L.-P. Hwang, J.H. Freed, Dynamic effects of air correlation functions on spin relaxation by translational diffusion in liquids, J. Chem. Phys. 63 (1975) 4017–4025.

[34] D. Sezer, M.J. Prandolini, T.F. Prisner, Dynamic nuclear polarization coupling factors calculated from molecular dynamics simulations of a nitroxide radical in water, Phys. Chem. Chem. Phys. 11 (2009) 6626–6637.

[35] I. Al-Bala'a, R.D. Bates, Effects of partially fluorinated hydrogen donors on ESR spectra in studies of hydrogen-bonded transient solvent–solvent complexes, J. Magn. Reson. 78 (1988) 271–280.